Journal of
Synchrotron
Radiation

ISSN 1600-5775

Received 7 July 2013
Accepted 27 November 2013

Characterization, optimization and surface physics aspects of *in situ* plasma mirror cleaning

Eric Pellegrin,[a]* Igors Šics,[a] Juan Reyes-Herrera,[a] Carlos Perez Sempere,[a] Juan Josep Lopez Alcolea,[a] Michel Langlois,[a]‡ Jose Fernandez Rodriguez[a]¶ and Vincent Carlino[b]

[a]Experiments Division, CELLS-ALBA, Carretera BP1413, km 3.3, Cerdanyola del Valles, Barcelona 08290, Spain, and [b]ibss Group Inc., 1559B Sloat Blvd, Suite 270, San Francisco, CA 94132, USA. *E-mail: epellegrin@cells.es

Although the graphitic carbon contamination of synchrotron beamline optics has been an obvious problem for several decades, the basic mechanisms underlying the contamination process as well as the cleaning/remediation strategies are not understood and the corresponding cleaning procedures are still under development. In this study an analysis of remediation strategies all based on *in situ* low-pressure RF plasma cleaning approaches is reported, including a quantitative determination of the optimum process parameters and their influence on the chemistry as well as the morphology of optical test surfaces. It appears that optimum results are obtained for a specific pressure range as well as for specific combinations of the plasma feedstock gases, the latter depending on the chemical aspects of the optical surfaces to be cleaned.

Keywords: synchrotron optics; carbon contamination; low-pressure RF plasma; X-ray photoemission spectroscopy; optical emission spectroscopy; interference microscopy.

1. Introduction

The basic approaches presently known regarding synchrotron optics cleaning procedures include *ex situ* as well as *in situ* set-ups, all of them using either oxygen radicals, hydrogen radicals or ozone as chemically active cleaning agents. Among the *ex situ* set-ups, UV lamps are used as ozone generators and efforts are now being made to integrate these lamps inside the vacuum chambers in order to avoid mirror extraction and subsequent bakeout. From an ozone generation efficiency point of view, these processes must be performed at oxygen partial pressures of ~100 mbar or higher, which classifies this method among the high-pressure approaches balancing ozone production efficiency against mean free path lengths.

For the low-pressure (*i.e.* less than 0.1 Torr or 0.133 mbar) *in situ* set-ups, most applications so far have been using a wide variety of various types of plasma sources as well as commercial components. Nevertheless, a basic distinction can still be made between the basic types such as (i) DC discharge and (ii) RF plasma sources, where the latter include both capacitive as well as inductively coupled plasma sources.

An even larger variety of cleaning procedures unfolds when it comes to the definition of plasma cleaning parameters such as feedstock gases, (partial) gas pressures, dynamic *versus* static gas supply modes, as well as cleaning processes based on kinetic and/or chemical effects. Obviously, in the present case aimed at the cleaning of optical elements only, plasma procedures excluding kinetic effects on the optical surfaces to be remediated have been selected. Also, approaches including the addition of water vapor to the feedstock gas have been omitted in view of maintaining the integrity of the ultra-high vacuum conditions of the vacuum chambers involved.

From an application point of view, the above diversity has led to a considerable amount of different approaches within the synchrotron and the EUV communities during the last decades, which are difficult to compare due to the above multitude of inherent degrees of freedom. Last but not least, the complexity of plasma physics and the associated diagnostics have so far resulted into a poor plasma process control and, consequently, to a poor understanding of the physics and surface chemistry involved in the cleaning process. Some 'voodoo' approaches that are currently being used in practical synchrotron life are basically a result of this situation.

The present study is an attempt to gain some better insight into the RF plasma cleaning process and thus to obtain a better control on the process parameters in view of safer and more efficient cleaning processes. This should also allow for the inclusion of other reflective coatings than gold, especially in the case of UV/VUV/XUV beamlines with a high sensitivity with respect to carbon contaminations, in view of keeping the flexibility required during the beamline design phase for achieving an optimum beamline performance.

‡ Present address: ESRF, 6 Rue Jules Horowitz, BP 220, 38043 Grenoble Cedex 9, France.
¶ Present address: Fusion For Energy, 2 Josep Pla, 08019 Barcelona, Spain.

2. Systematic approach

The systematic approach that has been chosen for the present study is based on the combination of the following basic elements: (*a*) cleaning test objects, (*b*) RF plasma guns, and (*c*) plasma feedstock gases.

2.1. Test objects

Three types of test objects have been used, depending on the type of data/characteristics to be obtained: (i) quartz micro-balance crystals for the determination of cleaning rates, (ii) metal foils for the determination of surface chemistry aspects during the cleaning process, and (iii) Au-, Rh- or Ni-coated single-crystalline Si substrates polished to optical quality for the determination of changes of the surface morphology during the cleaning process. All these latter mirrors were provided with a Cr binding layer between the Si substrate and the reflective coating.

Due to the practical problems associated with the availability of carbon coatings as deposited by the synchrotron beam, all the above test objects were (partially) coated with an amorphous sp^2/sp^3 carbon thin film with a thickness between 50 and 200 nm using a commercial e-beam evaporator with polycrystalline graphite target material (see supporting information for details[1]).

2.2. Low-pressure RF plasma guns

In order to explore the performance of different RF guns working in the pressure range between 0.001 mbar and 1 mbar, we have been using two different types of RF guns.

In a first approach, a custom-made 'traditional' capacitive coupling plasma (CCP) RF gun similar to the set-up described by Eggenstein *et al.* (2001) has been used, consisting of an RF amplifier operating at 13.56 MHz with an output power of up to 100 W, an automatic matching network unit for adapting the impedance of the amplifier to that of the antenna, and a cylindrical in-UHV aluminium antenna coupled to the in-air RF circuitry *via* an electrical vacuum feedthrough. Due to the internal electrical set-up of the RF matching unit and the above capacitive-coupling of the antenna, a negative DC bias voltage of up to several hundreds of volts is generated at the antenna during plasma operation resulting from the inherent kinetic properties of the plasma. This may lead to sputtering phenomena on the antenna material that will be discussed later.

In a second approach, a commercial RF gun (model GV10x 'Downstream Asher', IBSS, San Francisco, CA, USA) using an inductively coupled plasma (ICP) has been used. The Downstream Asher operation principle of that RF plasma source is different from the above traditional CCP source in a sense that it generates the plasma in a separate volume upstream from the chamber with the objects to be cleaned, with a small orifice between the plasma chamber and the cleaning chamber. This allows for an operation of the plasma chamber at higher pressures (corresponding to the plasma operation pressure regime) with the cleaning chamber at lower pressures (compatible with a larger reactant mean free path length), which stipulates dynamic gas supply as the only operation mode for the GV10x plasma source. In addition, the pressure gradient across the orifice results in a plasma jet between the two chambers, thus facilitating the distribution of the chemically active species across the cleaning chamber volume. Last but not least, the fact that the primary RF coupling coil is located outside the plasma volume results in chemically clean plasma free from any metallic sputtering products that would be generated by an in-vacuum antenna as in the case of a CCP source.

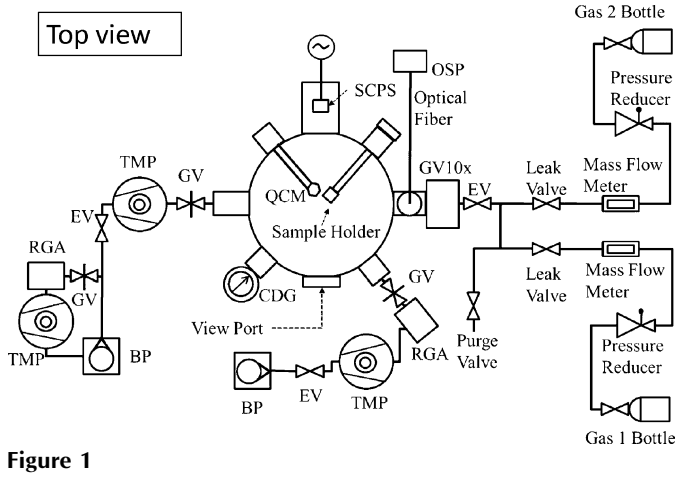

Figure 1
Conceptual layout of the RF test cleaning chamber (G10Vx: ICP plasma source; SCPS: small traditional plasma source; OSP: optical spectrometer; QCM: quartz crystal monitor; CDG: capacitive diaphragm gauge; GV: gate valve; TMP: turbomolecular pump; EV: electro valve; RGA: residual gas analyzer; BP: backing pump).

The front parts of both the CCP and the ICP sources were installed at a distance of 380 mm from the object(s) to be cleaned with the latter being located at the center of the cleaning chamber (see Fig. 1).

2.3. Gas mixtures

The obvious choice for the plasma feedstock gas for carbon cleaning/etching has traditionally been oxygen, thus using the oxygen radicals created by the plasma as chemically active oxidizing agents. Early studies used water vapor or argon as additional feedstock gases (Gibson, 1985; Johnson & Garrett, 1988), where the former can be considered as a contributor of hydrogen radicals acting as reducing agents during the cleaning process. On the other hand, argon gas is used for starting as well as for stabilizing the plasma discharge due to its inherently low breakdown voltage. Argon may also play a chemically active role for the carbon removal reaction and for the transport of reactive gas species as will be shown for the plasma cleaning processes using hydrogen/argon gas mixtures.

Here, we have used oxygen as well as oxygen/argon mixtures as feedstock gases for the oxidizing plasma. For the reducing plasma, different mixtures of hydrogen and argon, sometimes together with neon as a tracer gas for optical atom

[1] Supporting information for this paper is available from the IUCr electronic archives (Reference: PP5040).

actinometry (Lieberman & Lichtenberg, 2005), have been used.

Expanding the choice of feedstock gases was partly motivated by the assumption that non-noble metals used for reflective coatings would most probably be chemically altered (or oxidized) by the oxygen plasma, thus trading in carbon contaminations for an equally non-desirable oxide layer. In addition, it has been reported that blank Si optical surfaces have shown a decrease in reflectivity after long-term oxygen plasma treatments (M. Thomasset, private communication). This indicates a modification of the surface micro-roughness beyond a chemical modification as a function of an excessive plasma processing time.

The feedstock gas was supplied either in dynamic mode (*i.e.* with a continuous supply of fresh gas from the gas supply system together with a continuous pumping of the cleaning chamber) or in static gas supply mode. For the latter, starting from the evacuated chamber in the low 10^{-8} mbar pressure range the pumping system was valved off, the chamber filled with the gas mixture up to the desired (partial) pressure levels, and the plasma cleaning process was started.

Table 1
Cleaning rates in Å min^{-1} as obtained using the large traditional CCP RF gun using different oxygen partial pressures and RF powers.

Bold values indicate the maximum cleaning rate obtained.

	Static gas supply mode				Dynamic gas supply mode	
RF power	0.3 mbar	0.1 mbar	0.01 mbar	0.003 mbar	0.1 mbar	0.01 mbar
11 W	–	0.03	0.03	–	–	0.03
33 W	–	0.35	0.9	–	0.02	0.38
100 W	1.22	0.74	2.35	**3.7**	0.44	1.53

3. Experimental

Details on the experimental set-up as well as on equipment and procedures being used are available in the supporting information.

4. Results

4.1. Results from O_2 plasma cleaning with custom RF guns including capacitive coupling

In Fig. 2 we show some typical cleaning curves (*i.e.* the decrease of the carbon layer thickness on the microbalance quartz crystals as a function of cleaning process time) resulting from various cleaning runs using the large traditional CCP RF gun with different process parameters such as dynamic *versus* static gas supply mode, oxygen partial pressures and RF power input.

Cleaning trends that can be directly derived from these graphs are an increasing cleaning rate with increasing RF power and decreasing oxygen partial pressure, where the latter is limited by the lower pressure limit of about 0.001 mbar at which the RF plasma collapses. In addition, it can be noted that larger cleaning rates can be obtained using static gas supply conditions (including regular O_2 refills, see below) as compared with dynamic gas supply conditions. The measured cleaning rates range from 0 Å min^{-1} up to 1.53 Å min^{-1} and 3.7 Å min^{-1} for dynamic and static gas supply, respectively. Table 1 summarizes the carbon cleaning rates obtained for the various process parameters.

As already observed in previous studies (XEI Scientific Technical Report, Redwood City, CA 94063, USA), at the very beginning of the cleaning process an increase of the layer thickness can be observed that is attributed to the formation of adsorbed CO and CO_2 species onto the carbon layer surface. However, once an effective cleaning process sets in, this initial phenomenon is quickly superseded by the resulting thickness decrease.

In Fig. 3 we show the residual gas analyzer (RGA) time trends for selected residual gas masses as obtained from the

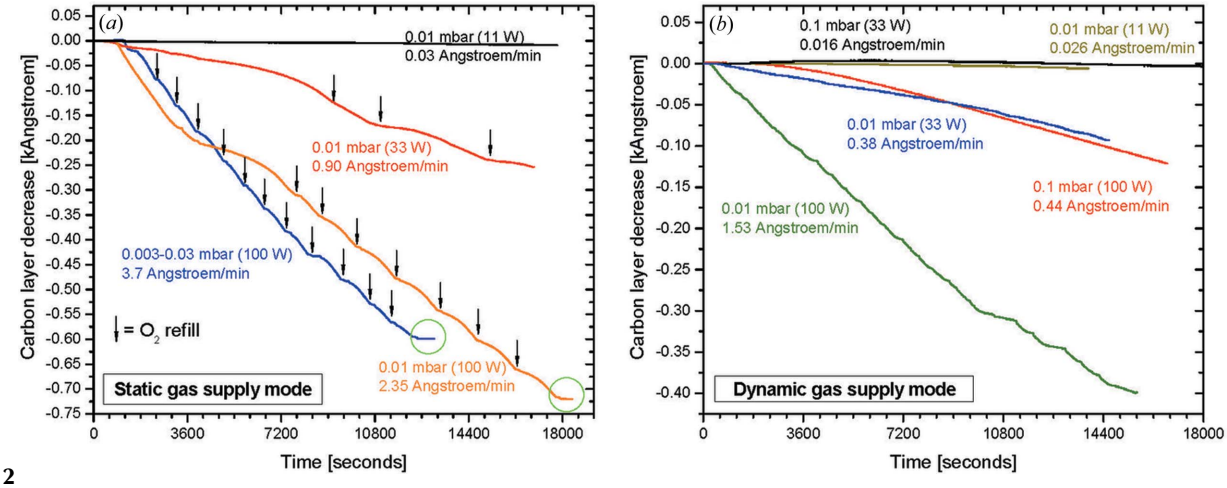

Figure 2
Typical cleaning curves obtained using the large traditional CCP RF gun in conjunction with an oxygen RF plasma. (*a*) Cleaning in static gas supply mode, (*b*) cleaning in dynamic gas supply mode. The vertical black arrows in (*a*) represent the O_2 gas refills. Pressure and power figures indicate the different process parameters in terms of oxygen partial pressure and RF power, respectively. Green circles represent the end point of the cleaning process when the carbon coating on the QCM crystals is completely removed.

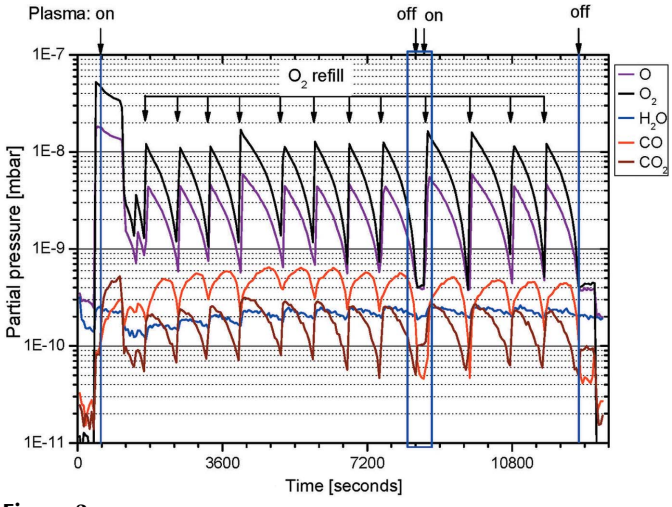

Figure 3
RGA time scan corresponding to the blue curve in Fig. 2(*a*) with a cleaning rate of 3.7 Å min^{-1}, static gas supply mode. Blue vertical lines indicate the start/stop of the RF plasma.

static cleaning process at 100 W RF power and a low oxygen partial pressure of 0.003 bar resulting in the highest cleaning rate of 3.7 Å min^{-1} [*i.e.* blue curve in Fig. 2(*a*)]. The overall time trends show the typical saw-tooth pattern for a static cleaning run, where fresh oxygen gas has to be supplied in regular time intervals due to the decrease of the total pressure as a function of time in order to provide sufficient oxygen for the cleaning process as well as to prevent a plasma collapse. This already indicates a substantial reaction rate of oxygen gas inside the plasma which is incommensurate with the small amount of carbon on the cleaning test object and that can be related to reaction processes on the Al RF antenna itself. In addition, considering the large changes at relatively large absolute partial pressures in the case of O_2 and atomic O with the small changes for CO_2 and CO at much lower partial pressures, the turnover between oxygen and carbon oxide gas species gives further evidence for the Al antenna as the main reactor for oxygen inside the plasma volume as compared with the carbon layer on the test object.

After the initial injection of O_2 gas up to the desired total pressure level and ignition of the plasma, one can observe in Fig. 3 a drop of the molecular O_2 and atomic O partial pressures, coinciding with a steep increase of masses 28 (CO) and 44 (CO_2), with the mass 28 partial pressure well beyond the (mostly N_2-related) levels before starting the plasma. This gives direct evidence for the conversion of carbon by the chemically active oxygen species into CO and CO_2, in conjunction with a corresponding decrease of the O_2 and O partial pressures due to the oxidation process. Interestingly, the CO partial pressure (mass 28) is higher than that of CO_2 (mass 44) which indicates that CO is stabilized in the plasma as compared with the usually more stable CO_2 oxidation end product. This could be shown by an inversion of the CO to CO_2 ratios when switching off the plasma (time period from 2 h 15 min to 2 h 18 min; see blue frame in Fig. 3). Thus, from a qualitative point, the time dependence of masses 32 (O_2), 16 (atomic O) and 28 (CO) do correspond with what is expected for the carbon conversion process. However, the overall decrease of *all* partial pressures towards the end of a single O_2 gas fill points towards an oxygen reaction process on the surface of the Al RF antenna in addition to the carbon conversion process mentioned above. This makes a quantitative analysis of the spectra for a detailed analysis of the carbon reaction processes difficult.

Fig. 4 shows the UV/VIS spectra of a short oxygen plasma cleaning run in static gas supply mode, using 75 W RF power at an oxygen partial pressure of 0.03 mbar. The UV/VIS spectrum basically consists of two major subsets [SpecLine software (Plasus GmbH, Kissing, Germany), using the databases from the following references: Kurucz (1995), NIST (1999), Striganov & Sventitskii (1968), Wiese *et al.* (1966, 1969), Pearse & Gaydon (1976), Crosswhite (1972); see also Shpilman *et al.*, 2008; Rosenberg & Crossley, 1988]: (i) a first set of emission lines in the wavelength range roughly between 250 and 500 nm originating from CO- and CO_2-related species, (ii) a second set of emission lines between 500 and 700 nm related to O^{2+} atomic species, as well as (iii) a third set consisting of two emission lines between 700 and 900 nm associated with the OI (or $O^{\bullet}$) radical (Rosenberg & Crossley, 1988; Pearse & Gaydon, 1963). This assignment matches well with the observation that in the initial phase of a cleaning run the plasma exhibits a yellow–greenish color, whereas a plasma in its later stages shows a blue color of the emitted light. The prominent lines beyond 700 nm wavelength within the top spectra in Fig. 4 (taken at the beginning of a cleaning run) can be seen at 777.2 and 844.6 nm and are associated with the $3p^5P$–$3s^5S$ and $3p^3P$–$3s^3S$ transitions of neutral oxygen OI (or $O^{\bullet}$) radical species, respectively. A more detailed analysis of the strong emission line at about 777.2 nm using a VUV

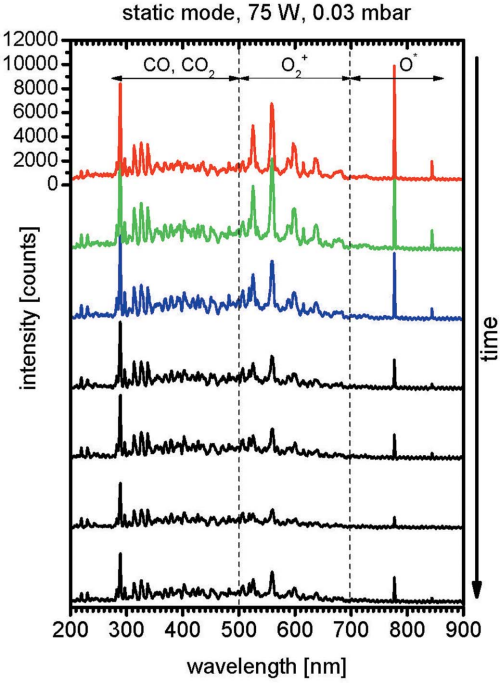

Figure 4
UV/VIS spectra taken during an oxygen plasma cleaning run using the small CCP traditional plasma source in static mode with 75 W RF power at 0.03 mbar process in 5 minute time intervals.

spectrometer with higher resolution reveals that this line actually consists of three lines that can be associated with the above $3p^5P–3s^5S$ transitions, but between different quantum numbers.

The main observation regarding the time dependence of these UV/VIS spectra taken in static gas supply mode is the decrease of the lines associated with the neutral OI (or O•) radical species at 777.2 nm and 844.6 nm as a function of time, indicating the consumption of this atomic oxygen species during the carbon cleaning process in accordance with the results from the time dependence of the RGA spectra. This OI depletion, together with the reaction of the oxygen radicals on the surface of the Al RF antenna, explains in some more detail why in the case of static gas supply a regular refill of the plasma volume with O_2 gas is required for keeping the cleaning process up.

In Fig. 5 we show the results from an X-ray photoelectron spectroscopy (XPS) analysis of noble metal foils (Au, Ni and Rh) after carbon deposition and subsequent oxygen plasma cleaning using a small traditional CCP RF gun. Although a visual inspection of the metal foils after the cleaning process resulted in an apparently complete carbon removal, all the XPS spectra in Fig. 5 give evidence of an incomplete cleaning due to the C1*s* and O1*s* core level lines that still show a substantial intensity as compared with the metal core level lines. On the upside, although there are obviously sputtering processes occurring at the surface of the capacitive coupled Al antenna inside the cleaning chamber (due to the negative static charging of the capacitive coupled antenna up to several hundreds of volts), the XPS spectra do not give any evidence of a foreign metal contamination of the foils' surfaces. This may well be attributed to the chosen geometrical arrangement that excludes a direct line of sight between the plasma source and the test object. Nevertheless, there is obviously still some room for improvement regarding the complete cleaning of the surfaces involved.

4.1.1. Discussion. The effect of the increasing cleaning rate with increasing RF power as shown in Fig. 2(*a*) can be readily understood by an increased generation of oxygen radicals at a given oxygen partial pressure. This will be discussed in more detail in the framework of the GV10x plasma source.

On the other hand, the enhanced cleaning rate at lower oxygen partial pressures can be explained by an increase of the oxygen radical mean free path length, making a larger amount of oxygen radicals available for the carbon oxidation instead of recombining to O_2 molecules as could be observed from the increase of the ratio of atomic O partial pressure over molecular O_2 partial pressure in the RGA spectra for static mode.

The lower cleaning rates obtained for the dynamic gas supply mode as compared with the static supply mode are due to the inherently lower production rate of oxygen radicals using the traditional RF guns. This could be shown by the enhanced $O^•/O_2$ partial pressure ratios for the cleaning runs in static mode as measured by the RGA.

Summarizing the discussion using traditional RF guns, these devices do not offer the performance that would be expected

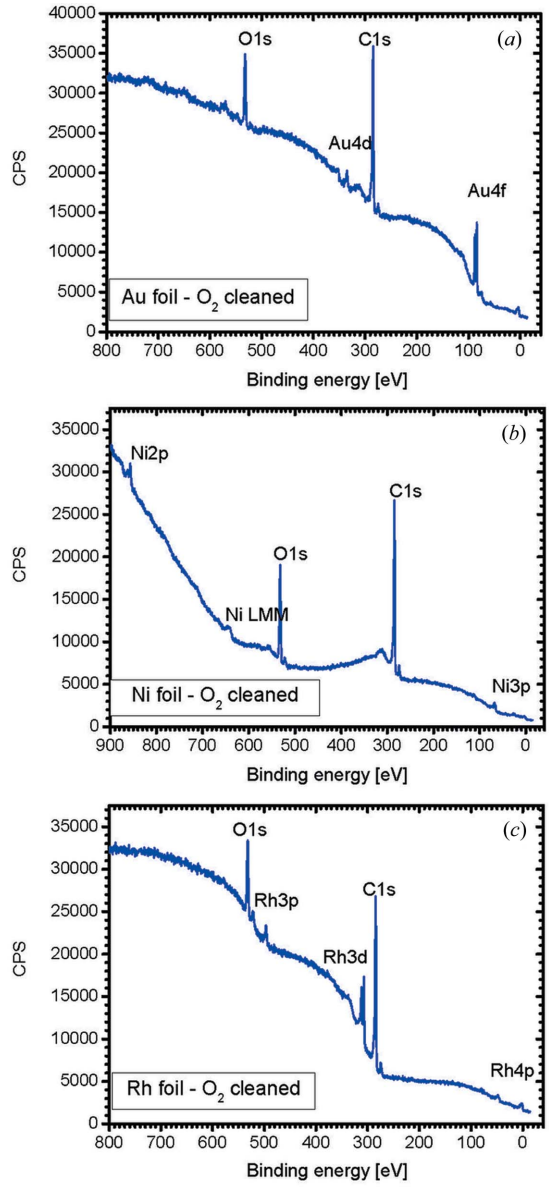

Figure 5
XPS spectra from Au (*a*), Ni (*b*) and Rh (*c*) foils after carbon contamination and subsequent oxygen RF plasma cleaning using the small traditional CCP RF gun.

in terms of cleaning efficiency and thoroughness. Regarding the latter, one has to keep in mind that the surface sensitivity of XPS measurements is obviously much more pronounced as compared with the reflectivity of soft X-ray photons determined by the large(r) photon penetration depth. 'At-wavelength' measurements of the reflectivity would be required in order to settle this issue quantitatively, but there is clearly some room for improvement as far as the efficiency of the cleaning process is concerned.

4.2. Results from O_2 and O_2/Ar plasma cleaning using a GV10x RF gun including inductive coupling

In Fig. 6 we show the carbon cleaning curves obtained by using the GV10x ICP source with either pure oxygen or

Table 2
Cleaning rates in Å min^{-1} as obtained using the GV10x ICP RF gun using various oxygen-based feedstock gases, RF power levels and total pressures.

Bold values indicate the maximum cleaning rate obtained.

	Pure O_2 feedstock gas		96% O_2 and 4% Ar feedstock gas	
RF power	0.01 mbar	0.005 mbar	0.01 mbar	0.005 mbar
25 W	0.46	–	1.2	–
50 W	2.28	–	2.3	–
98 W	4.93	8.43	5.8	**11.6**

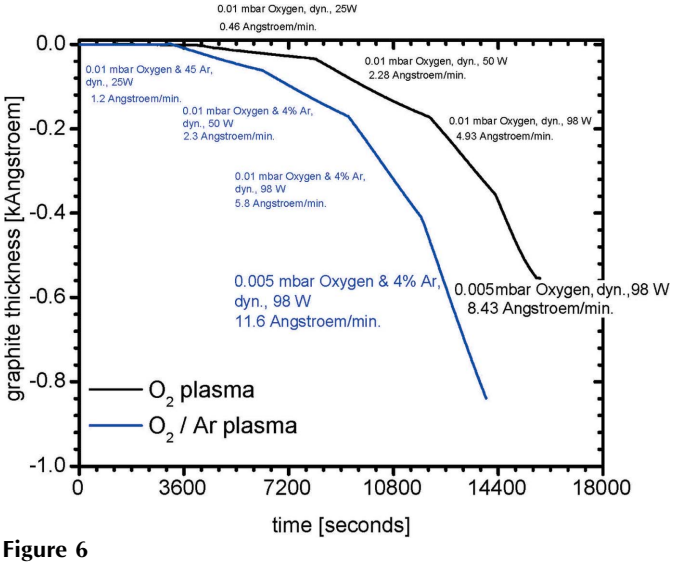

Figure 6
Cleaning curves obtained using an oxygen RF plasma produced by the GV10x RF gun.

oxygen (96%)/argon (4%) feedstock gas mixtures at various total pressures and RF powers. Due to the inherent geometry of this plasma source mentioned above, these cleaning runs were performed in dynamic gas supply mode in order to allow for a plasma stream from the plasma chamber into the cleaning chamber through the orifice separating these two volumes. Table 2 gives an overview of the carbon cleaning rates achieved using different process parameters.

Comparing the cleaning rates given in Table 2 with those given in Table 1, it is clear that the cleaning speeds achieved with the GV10x gun are higher by a factor of two to three. This coincides with other observations regarding the different runs and will be discussed in more detail later. Another aspect is the increase of the cleaning rates by introducing Ar into the feedstock gas mixture.

The optical emission spectra (OES) taken just downstream of the GV10x ICP source inside the cleaning chamber at a RF power of 50 W and an oxygen partial pressure of 0.012 mbar are shown in Fig. 7. As in the case of the OES from the traditional RF gun shown in Fig. 4, the typical molecular and atomic oxygen lines at wavelengths beyond 700 nm can be seen that include the pronounced lines at 777.2 nm and 844.6 nm from neutral atomic radical oxygen $O^{\bullet}$ species as well as the weaker lines from O^{2+} molecules between 500 and

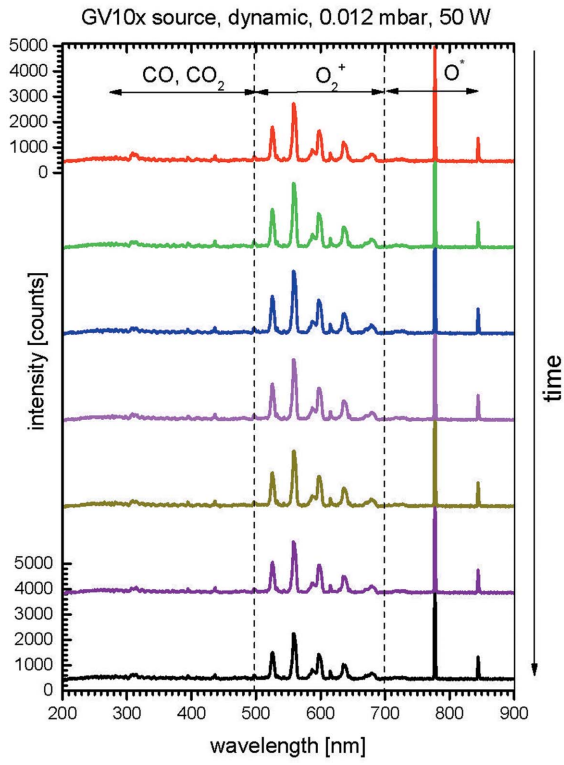

Figure 7
UV/VIS plasma emission spectra taken during an oxygen plasma cleaning run using the GV10x ICP RF gun with 50 W RF power in 20 minutes time intervals.

700 nm. However, the lines between 200 and 500 nm due to CO- and CO_2-species that had a significant intensity in the traditional RF gun spectra are not present in the GV10x data in Fig. 7. This is attributed to the fact that the latter runs were performed in dynamic gas supply mode whereas the former spectra were taken under static conditions, where the CO and CO_2 products from the carbon cleaning process stay within the plasma. Moreover, what can also be observed from Fig. 7 is the *constant* intensity from the above two lines related to $O^{\bullet}$ species, being of importance for the carbon cleaning process, throughout the duration of the experiment.

The XPS spectra from pristine as well as from carbon-contaminated and subsequently oxygen-plasma-cleaned Au, Ni and Rh metal foils are shown in Figs. 8, 9 and 10, respectively. Taking a closer look at the differences between the Au foil spectra in Fig. 5(*a*) (cleaned with small traditional CCP RF gun) and Fig. 8(*a*) (cleaning with GV10x ICP Downstream Asher), it becomes obvious that the carbon cleaning in the case of the GV10x gun is much more efficient. This can be easily seen from the lower background intensity as well as from the lower intensity of the O1*s* and C1*s* XPS lines as compared with the inherent Au XPS lines in Fig. 8. This finding actually holds for all the metal foil spectra shown in Fig. 5 as compared with the spectra in Figs. 8, 9 and 10. It has to be noted that the intensity of the C1*s* XPS line for the processed foil in Fig. 8(*c*) is lower than that of the pristine foil, which provides evidence of a complete cleaning of the formerly carbon-covered Au foil.

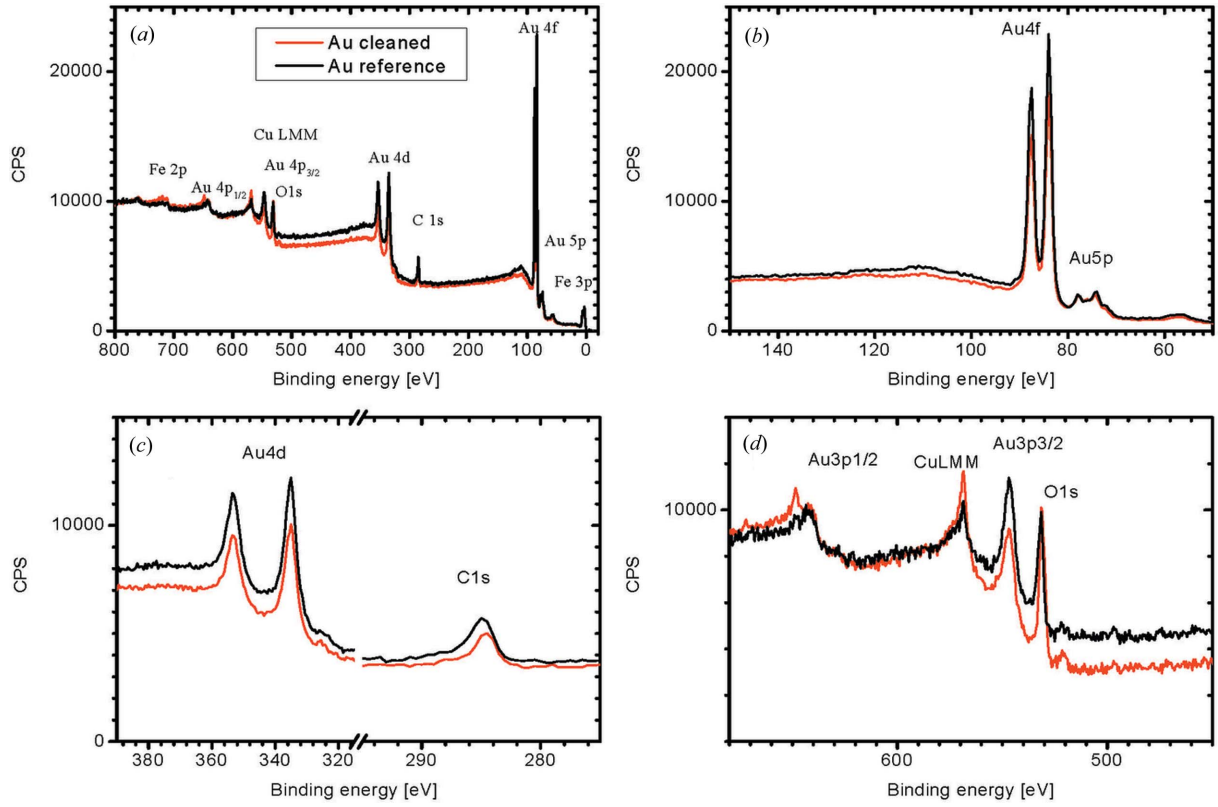

Figure 8
XPS spectra from a pristine Au foil (black lines) as well as from a Au foil after carbon contamination and subsequent oxygen RF plasma cleaning using a GV10x ICP RF gun (red lines).

Besides the expected core level lines (*i.e.* Au, Ni, Rh, O, C), the XPS overview spectra in Figs. 8(*a*), 9(*a*) and 10(*a*) show some weak lines associated with Fe and Cu as foreign materials. Since these trace materials can be partly related to metallic impurities remaining from the foil manufacturing and/or handling and, most importantly, do not change in intensity when going from the pristine to the plasma-processed metal foils, it can be concluded that also in the case of the GV10x ICP Downstream Asher the cleaning process does not result in any contamination of the surfaces to be cleaned.

We now discuss the XPS spectra in more detail. Focusing on the Au spectra in Figs. 8(*b*)–8(*d*), there are almost no changes regarding shape and binding energy (BE) of the Au XPS lines. This shows that, as can be expected, Au as a noble metal remains chemically unaffected by the oxygen plasma treatment. This picture drastically changes when going to the Ni XPS spectra in Fig. 9. The Ni 2*p* reference spectrum of the pristine Ni foil in Fig. 9(*b*) (black line) shows the well known XPS satellite spectrum of Ni_2O_3 together with the sharp Ni $2p_{1/2}$ and Ni $2p_{3/2}$ lines of metallic Ni at lower BEs (Miller & Simmons, 1993). Looking at the XPS spectrum of the cleaned Ni foil (red line), it is evident that the sharp metallic Ni lines have almost disappeared whereas the multiplet lines of Ni_2O_3 (Mansour & Melendres, 1994) have increased in intensity. Also, the O1*s* XPS line for the cleaned Ni foil exhibits an additional shoulder at lower BE (about 529.2 eV) in addition to the main line at about 531.2 eV where the former and the latter are attributed to oxygen atoms in Ni_2O_3 and oxygen in conjunction with adventitious carbon, respectively. This provides evidence that the Ni foil with its native Ni_2O_3 layer is oxidized further by the oxygen/argon plasma, thus leading to a decrease of the Ni 2*p* lines related to metallic Ni. This interpretation is corroborated by XPS data on the thermal treatment of a Ni foil in an oxygen atmosphere where a thin Ni_2O_3 layer of up to 60 Å could be formed after heating to 673 K (Galtayries & Grimblot, 1999).

The XPS spectra from pristine and processed Rh foils in Fig. 10 also show an interesting change after the oxygen/argon plasma treatment. As mentioned above, there is no evidence for additional contamination of the foils by adventitious foreign metal atoms as can also be inferred from Fig. 10(*a*). However, there is an obvious increase in the intensity of the O1*s* line as well as a shape change of the Rh 3*d* lines by the cleaning process. Looking at the individual Rh 3*d* and O1*s* spectra in Figs. 10(*b*) and 10(*c*), there is a shift of the $Rh_{5/2}$ and the $Rh_{3/2}$ BEs to higher energies by 0.5 to 1 eV as well as a shift of the O1*s* line to lower BE by 1.5 eV. In addition, there is a strong change regarding the shape and the intensity of the Rh 3*d* XPS lines change by the cleaning process. By comparison with XPS data (Abe *et al.*, 2001) from Rh metal, Rh_2O_3 and RhO_2, it can be concluded that the oxygen plasma treatment leads to the formation of trivalent Rh^{3+} as in Rh_2O_3. It might seem somewhat surprising as Rh can be considered as a noble metal, thus being corrosion-resistant as in the above case of Au. However, previous work by Tolia *et al.* (1994) on the oxidation/reduction of Rh metal has shown that the oxidation

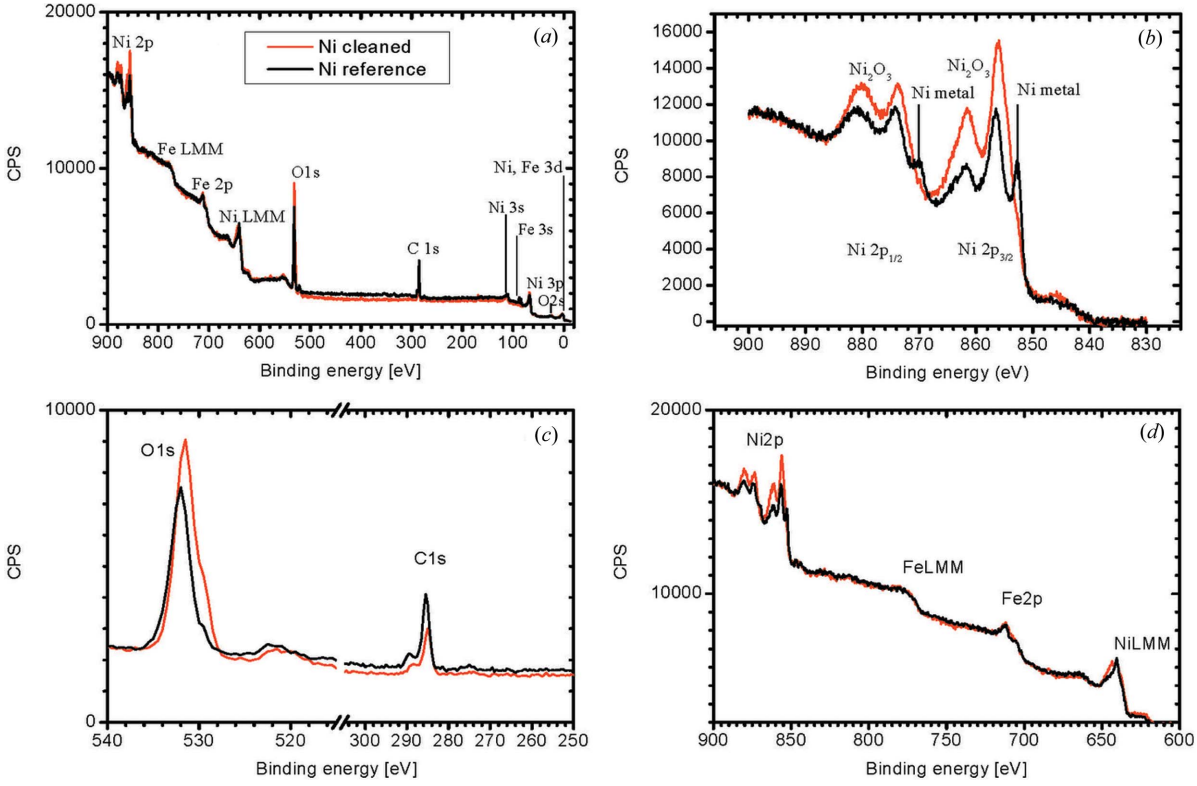

Figure 9
XPS spectra from a pristine Ni foil (black lines) as well as from a Ni foil after carbon contamination and subsequent oxygen RF plasma cleaning using a GV10x ICP RF gun (red lines).

of Rh can be initialized in an oxygen atmosphere at a relatively moderate temperature of 323 K, while a full oxidation requires sample temperatures as high as 573 K for an extended amount of time. Comparing the spectral shapes of our Rh 3*d* and O1*s* XPS lines with these data, we conclude that the present oxygen plasma-treated Rh foil corresponds to an intermediate regime where, after a thermal oxygen treatment between 423 and 523 K, both Rh metal and Rh_2O_3 do coexist. This leads to a broadening of the two-component Rh 3*d* XPS line (Rh metal and Rh_2O_3) as well as to the appearance of two O1*s* lines, where the low-BE line at 530.0 eV is assigned to Rh_2O_3 whereas the line at about 531.5 eV BE can be associated with either RhOOH or RhO_2. A summary of the XPS core level binding energies is given in Table 6.

Last but not least, we have performed an analysis of the effect of the oxygen plasma treatment on the micro-roughness of small test mirrors with Au, Rh and Ni reflective coatings using an interference microscope. First, micro-roughness measurements were performed on the pristine mirrors before performing any treatment. Then, one half of the mirror reflective surface of each mirror was provided with a carbon coating using our standard coating process. Finally, all mirrors were cleaned with pure oxygen plasma with a RF power up to 98 W at a total pressure of 0.01 mbar. Table 1 in the supporting information shows the results from these micro-roughness measurements for three test mirrors with different reflective coatings. As can be seen from these numbers, there is no increase of the micro-roughness (R_q) of the processed surfaces as compared with the pristine surfaces of slightly less than 0.2 nm r.m.s. and just beyond 0.2 nm r.m.s. One can thus even surmise a slight reduction of the micro-roughness when going from the pristine to the plasma-processed surfaces.

4.2.1. Discussion. The most prominent result regarding the oxygen plasma cleaning using the GV10x ICP RF gun as compared with the traditional RF gun is the increase in cleaning rate by a factor of two to three together with a more thorough/efficient cleaning, resulting in the conversion of the carbon-coated optical surfaces into surfaces with pristine properties, at least in the case of an Au optical coating.

The above improvements in terms of cleaning rate compared with the results from the traditional RF gun are probably due to a combination of three aspects:

(i) A more efficient and continuous supply of neutral OI (or $O^{\bullet}$) radicals to the cleaning process.

(ii) No 'self-intoxication' of the plasma by derivatives of CO or CO_2 species due to the removal of these carbon gas species by using the dynamic gas supply mode.

(iii) In the case of the Ar/O_2 gas mixtures a stabilization of the plasma by the Ar discharge. Moreover, there could be a photon-assisted breaking of carbon bonds and/or carbon oxidation as has already been observed in previous plasma experiments due to the optical wavelengths emitted by the Ar species (Fridman, 2008).

The increase in the neutral OI (or $O^{\bullet}$) radical production efficiency for the GV10x ICP gun as compared with the CCP RF gun can readily be observed from the intensity ratio of the line at 777.2 nm (representing the neutral OI radicals) as

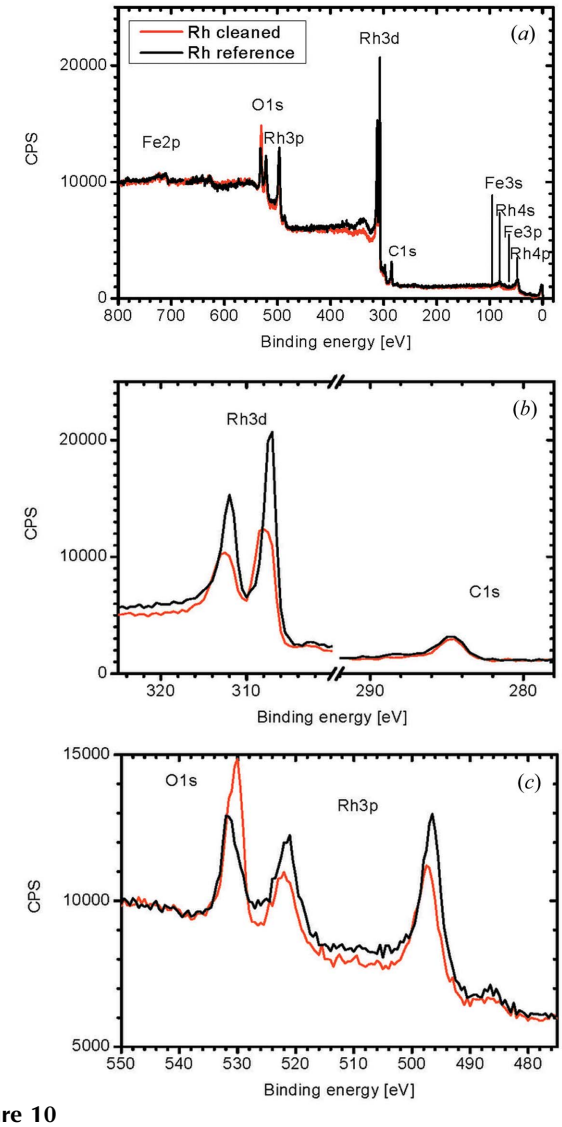

Figure 10
XPS spectra from a pristine Rh foil (black lines) as well as from a Rh foil after carbon contamination and subsequent oxygen RF plasma cleaning using a GV10x ICP RF gun (red lines).

compared with the line intensities in the wavelength rage between 500 and 700 nm in Fig. 11(*a*).

The continuous O• supply in the case of the GV10x gun is evident from the constant OI line intensities as already discussed for Fig. 7 in strong contrast to the decrease of these emission lines in between oxygen gas refills for the traditional CCP RF gun in Fig. 4. The absence of self-intoxication for the GV10x gun is also obvious from the absence of line intensities between 250 and 500 nm in Figs. 7 and 11(*a*) (red line).

In Fig. 11(*b*) we show the optical emission spectra for the cleaning runs shown in Fig. 6 for different process parameters while Fig. 11(*c*) shows the intensity of the OI emission line at 777.2 nm as a function of the achieved cleaning rate for the case of a pure O_2 plasma as well as 4% Ar/O_2 gas mixture (see Fig. 6). From this diagram it is evident that there is a correlation between the concentration of neutral O• radicals and the observed carbon cleaning rate. Interestingly, the admixture of Ar into the oxygen feedstock gas results in a reduction

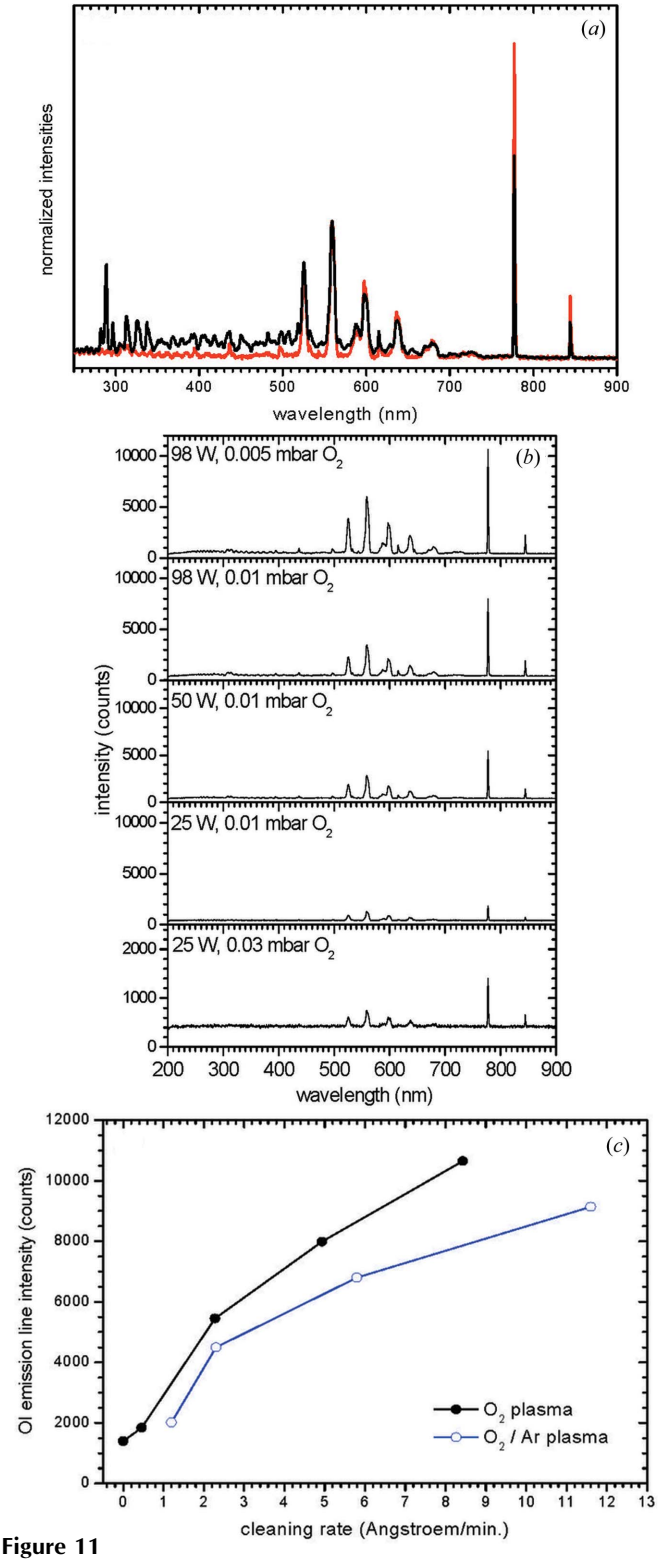

Figure 11
(*a*) UV/VIS spectra taken during an oxygen plasma cleaning run using the traditional CCP RF gun (black line, static mode, 0.03 mbar) as well as the GV10x ICP RF gun (red line, dynamic mode, 0.01 mbar) with 50 W RF power. The spectra have been normalized at the peak intensity at 559 nm. (*b*) UV/VIS spectra taken during the oxygen cleaning run in Fig. 6 using the GV10x ICP RF gun with different O_2 total pressures and RF powers. (*c*) Intensity of the OI emission line at 777 nm as a function of the carbon cleaning rate obtained using the different process parameters shown in Fig. 6 for pure O_2 plasma (black line, closed symbols) and a 4% Ar in O_2 gas mixture (blue line, open symbols).

Table 3
Cleaning rates in Å min^{-1} as obtained using the GV10x ICP RF gun with various hydrogen-based feedstock gases.

Bold values indicate the maximum cleaning rate obtained.

RF power	Pure H_2 feedstock gas	65% H_2, 5% Ar, 30% Ne feedstock gas	50% H_2, 20% Ar, 30% Ne feedstock gas
Total pressure	0.01 mbar	0.01 mbar	0.01 mbar
60 W	–	–	1.1
90 W	0.07	1.4	**1.6**

of the OI line intensity at a given cleaning rate, which indicates a more efficient transport of the fewer chemically active O• radicals to the test object to be cleaned. This specific feature of Ar as a carrier gas will show up again in the case of hydrogen/argon plasma.

Although the oxygen plasma in conjunction with the GV10x ICP gun offers a clear improvement in terms of cleaning rate and efficiency, the undesirable oxidation of Ni beyond the native Ni_2O_3 layer as well as the oxidation of Rh as a noble metal shows the limitations of the present approach and calls for alternatives that would allow for a cleaning of these metals without resulting in an oxidation of the surfaces. Interestingly, the oxidation process on Ni and Rh apparently does not have an impact on the micro-roughness of the surfaces involved indicating the formation of an oxide layer with a uniform growth rate and thickness.

4.3. Results from H_2/Ar plasma cleaning using a GV10x RF gun including inductive coupling

In view of avoiding oxidation phenomena that are inherent to the use of oxygen plasma, a second approach has been tested using the GV10x ICP RF gun together with H_2/Ar gas mixtures as a feedstock gas. This approach makes use of the fact that hydrogen radicals will reduce the carbon atoms in view of converting them into volatile hydrocarbon species such as ethane, methane *etc.* in a similar manner to commercial thermal plasma jets that are used for the production of acetylene from coal (Fridman, 2008). In the same vein, the reducing properties of hydrogen radicals would protect the optical surfaces from being oxidized during the cleaning process.

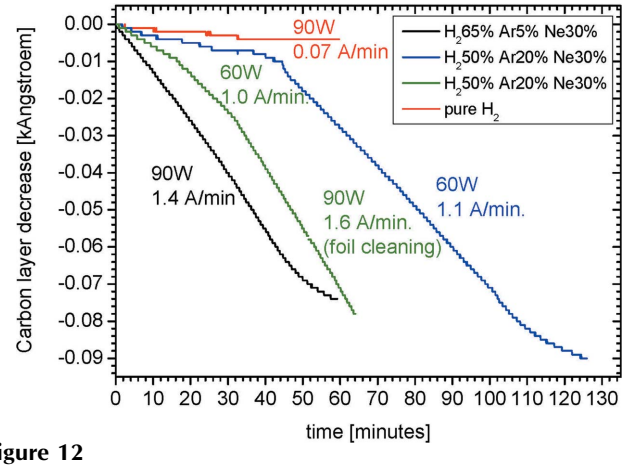

Figure 12
Cleaning curves obtained using a hydrogen/argon/neon RF plasma produced by the GV10x RF gun at a total pressure of 0.01 mbar.

Table 4
Cleaning rates in Å min^{-1} as obtained using the GV10x ICP RF gun using various hydrogen–argon feedstock gas mixtures at different total pressures at 99 W RF power.

Bold values indicate the maximum cleaning rate obtained.

Run number	Total pressure	H_2/Ar ratio	Cleaning rate	H-α intensity
1	0.01 mbar	10%/90%	0.85 Å min^{-1}	1500 counts
2	0.01 mbar	25%/75%	0.94 Å min^{-1}	1850 counts
3	0.01 mbar	50%/50%	0.42 Å min^{-1}	1560 counts
4	0.01 mbar	75%/25%	0 Å min^{-1}	600 counts
5	0.01 mbar	0%/100%	0.75 Å min^{-1}	0 counts
6	0.005 mbar	20%/80%	0.97 Å min^{-1}	1700 counts
7	0.0025 mbar	20%/80%	1.4 Å min^{-1}	1000 counts
8	0.0015 mbar	7%/93%	**1.7 Å min^{-1}**	600 counts

In Fig. 12 we show the results from the corresponding cleaning runs that also include neon as a tracer gas (for O atom actinometry) within the feedstock gas mixture. Table 3 summarizes the obtained cleaning rates.

As can be seen from the data in Fig. 12 and Table 3, the lowest cleaning rate of 0.07 Å min^{-1} is obtained when using pure hydrogen as a feedstock gas. With increasing argon concentration the cleaning rate increases and the same happens as a function of RF power. Comparing the data from Table 3 with those from Table 2, it is clear that the maximum cleaning rate obtained using hydrogen gas mixtures is reduced by almost one order of magnitude as compared with the maximum cleaning rate obtained from oxygen gas mixtures.

Since the gas mixing ratio appears to have a strong influence on the efficiency of the cleaning process, we have performed a further optimization of the hydrogen plasma cleaning including a wide variation of both the H_2/Ar mixing ratio as well as the total gas pressure. Table 4 shows the results from this test run, performed at a RF power of 99 W.

What can be derived from both Tables 3 and 4 is the fact that the highest cleaning rates (*e.g.* 1.7 Å min^{-1}) are observed for highest RF power (around 90 W) in conjunction with a low hydrogen admixture (*i.e.* 20% or less) and with a low total pressure in the 10^{-3} mbar range.

In Fig. 13 we show typical optical emission spectra taken during the cleaning runs listed in Table 4 that have also been used for verifying the H_2/Ar gas mixing ratios in addition to the ratio of gas partial pressures obtained while adjusting the gas supply. The emission peaks in the wavelength range from roughly 655 to 900 nm and 400 to 440 nm are due to the emission from Ar species whereas the peaks between 350 and 660 nm are mostly due to the emission from hydrogen species. The most intense emission lines are the well known H-α and H-β Balmer lines from neutral hydrogen radicals at 656.3 and 486.1 nm, respectively. For the Ar OES, one of the prominent lines at 750.4 nm corresponds to the the $3s^2 3p^5 4s$ to $3s^2 3p^5 4p$ transition. Whereas in the case of the oxygen/argon plasma cleaning there is a direct correlation between the concentration of O• radicals present in the plasma and the cleaning rate

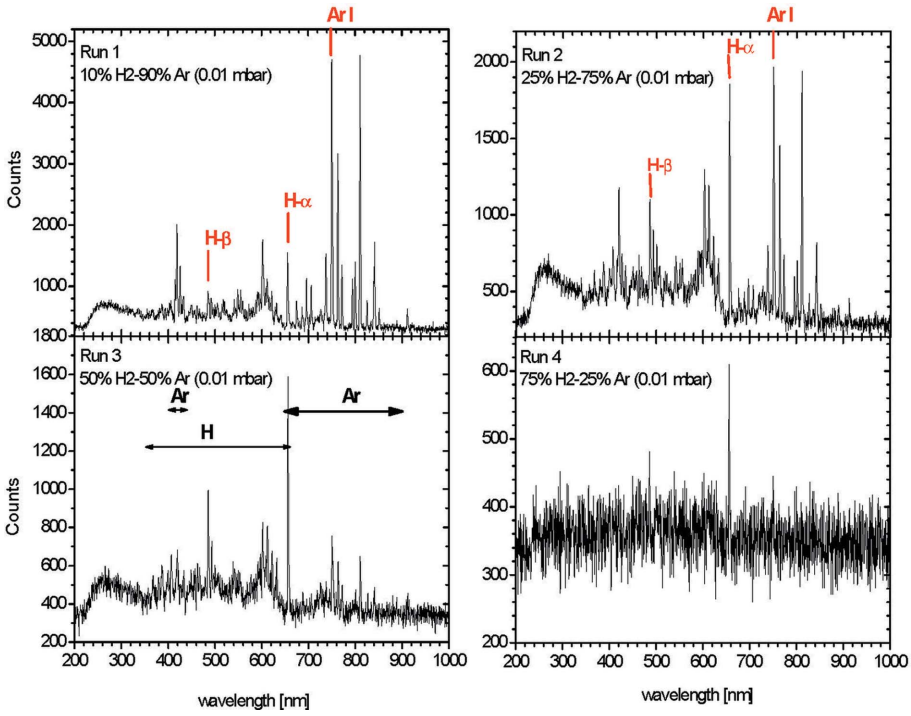

Figure 13
UV/VIS plasma emission spectra taken with different H_2/Ar gas mixtures using the GV10x ICP RF gun in dynamic mode with 99 W RF power for runs 1 to 4 (see Table 4).

(see Fig. 11*c*), the situation in hydrogen/argon plasma appears to be more complex when taking the intensity of the Balmer H-α line as a reference for the chemically active species regarding the carbon cleaning since it obviously does not scale with the carbon cleaning rate, but rather with the inverse total gas pressure (see runs 5 to 8 in Table 4). Again, the latter result points out the importance of the mean free path length, whereas the finding that a low but still significant carbon cleaning rate can be obtained from a pure Ar plasma (see run 5 in Table 4) again indicates an active role of the excited Ar species in the cleaning process. On the other hand, Ar sputtering processes that would explain the observed cleaning rate can be excluded since the quartz crystal sample is at ground, thus avoiding any DC charging and resulting sputtering phenomena.

In Figs. 14, 15 and 16 the XPS spectra of pristine and processed Au, Ni and Rh

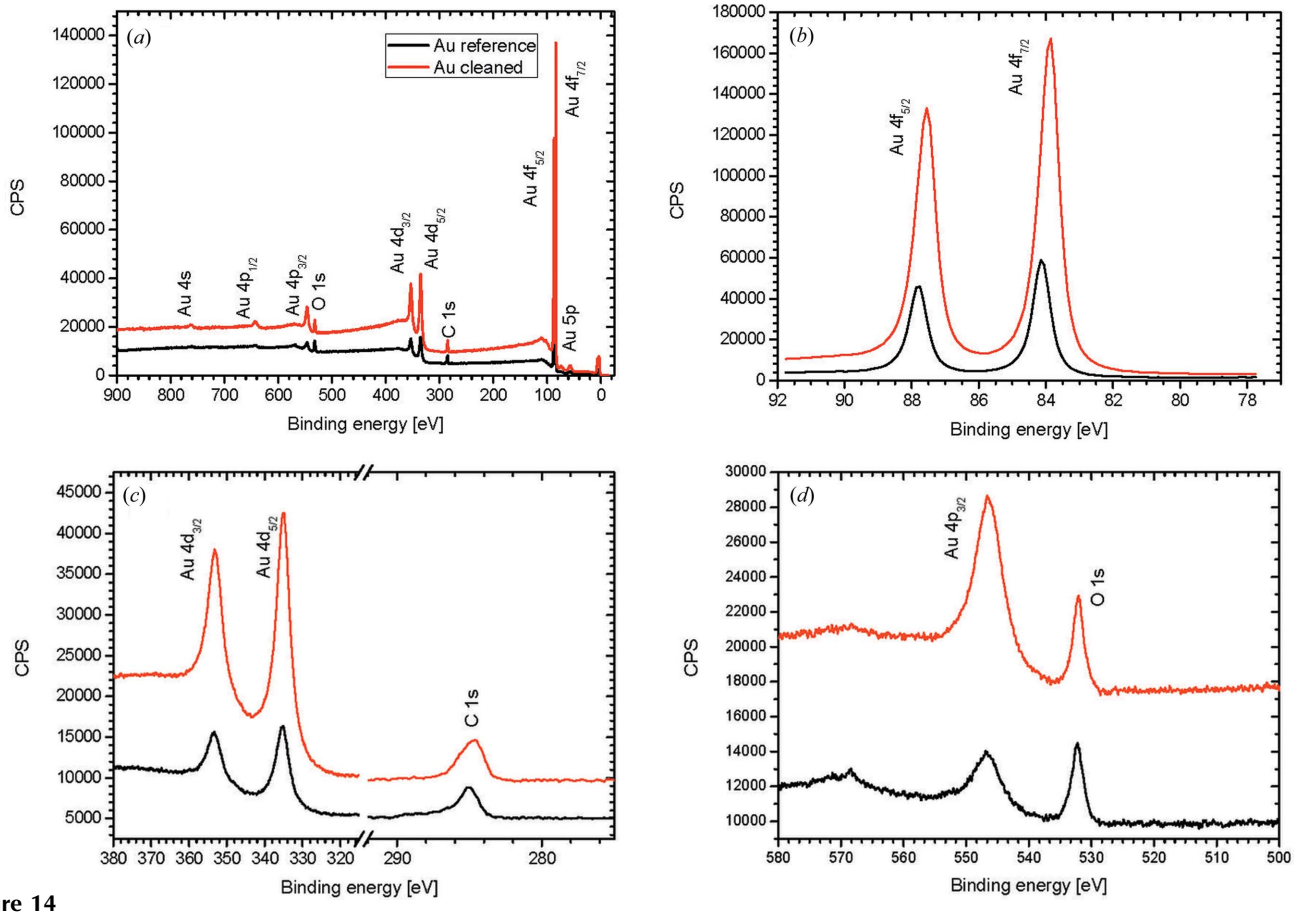

Figure 14
XPS spectra from a pristine Au foil (black lines) as well as from a Au foil after carbon contamination and subsequent hydrogen RF plasma cleaning using a GV10x ICP RF gun (red lines).

foils are shown as in the case of the previous RF plasma treatments. Comparing the evolution of the overview XPS spectrum in Fig. 14(*a*) as well as of the Au XPS lines in Figs. 14(*b*) and 14(*d*) as a function of the plasma treatment with the XPS data in Fig. 8, there is an apparent 'sharpening' (*i.e.* an increase of the peak intensity) of the Au XPS lines. As in the case of the Au foil processed in an oxygen plasma, there is no evidence for a change of surface contamination by foreign materials due to the plasma cleaning process that would result in a relative change between reference foil and the plasma-cleaned foil. Judging from the intensity of the O1*s* and C1*s* core level lines before and after the cleaning process, the cleaning efficiency appears to be as good as in the case of the oxygen plasma cleaning.

The most interesting part of the XPS analysis concerns the results for the Ni and Rh foils (see Figs. 15 and 16). For the Ni foil the Ni *LMM* Auger line as well as the Ni 2*p* line in the overview spectrum in Fig. 15(*a*) already provides evidence that there has been a significant change in the Ni foil surface chemistry. Having a closer look at the Ni 2*p* core level lines in Fig. 15(*b*), the pristine Ni foil shows the combination of a Ni 2*p* spectrum of metallic Ni together with the satellite XPS spectra of Ni_2O_3 as already shown in Fig. 9(*b*). After hydrogen/argon plasma processing, the two single Ni $2p_{1/2}$ and Ni $2p_{3/2}$ XPS lines of metallic Ni significantly increase in intensity as compared with the Ni_2O_3 lines, thus giving direct evidence of a partial reduction of the native Ni_2O_3 layer to metallic Ni. There is a slight increase of the Fe features which can either be attributed to the surface cleaning by the plasma (similar to a mild sputtering process, thus highlighting impurities pre-existing in the surface) or an increase in Fe contamination. This is difficult to distinguish at this point.

In the case of the XPS spectra for the Rh metal foils shown in Fig. 16, again the same line sharpening of the Rh 3*p* in Rh 3*d* core level lines as in the case of the Au foils can be distinguished, especially in Fig. 16(*c*). Moreover, a shift of the O1*s* line to lower BEs by about 0.5 eV can be observed (see Fig. 16*b*), whereas the Rh 3*p* as well as the Rh 3*d* BEs remain the same. This is in contrast to the findings for the oxygen plasma cleaned Rh foils (see Fig. 10*b*), where the oxidation did lead to a clear BE shift to higher energies. From the intensity of the O1*s* and C1*s* core level lines before and after the cleaning process, the cleaning efficiency appears to be as efficient as in the case of the Au foil. We thus conclude that Rh metal is inert with respect to hydrogen plasma cleaning which is in contrast to the above findings from the oxygen plasma cleaning for this noble metal. A summary of the XPS core level binding energies is given in Table 6.

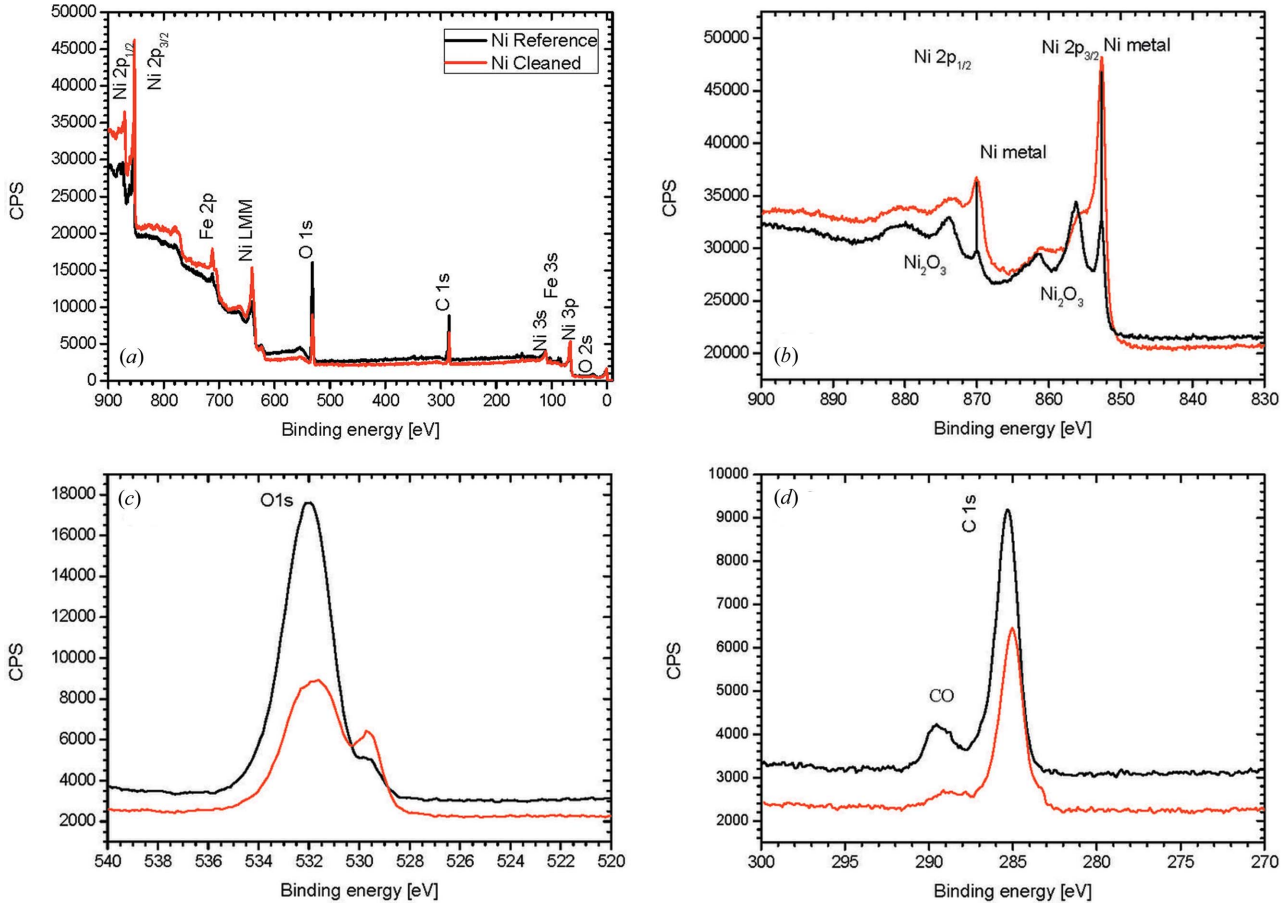

Figure 15
XPS spectra from a pristine Ni foil (black lines) as well as from a Ni foil after carbon contamination and subsequent hydrogen RF plasma cleaning using a GV10x ICP RF gun (red lines).

Again, in order to check for possible changes in the sample surface morphology as a function of the plasma processing, interference microscopy measurements have been performed on the same test mirrors with Au-, Rh- and Ni-coated optical surfaces before and after the hydrogen plasma cleaning. The plasma cleaning process parameters were chosen to be the ones from Fig. 12 with the highest cleaning rate (90 W RF power, 0.01 mbar total pressure, 50% hydrogen, 20% argon, 30% neon, dynamic gas supply mode). Results are shown in Table 2 of the supporting information. As in the case of the oxygen plasma cleaning in Table 1 of the same document, there are no significant changes regarding the micro-roughness figures (staying just below 0.2 nm r.m.s.) that would indicate a roughening of the optical surface by the cleaning process. This gives additional evidence for the safe aspects of all the cleaning processes performed so far using the GV10x ICP gun as far as the morphology of the optical surfaces is concerned.

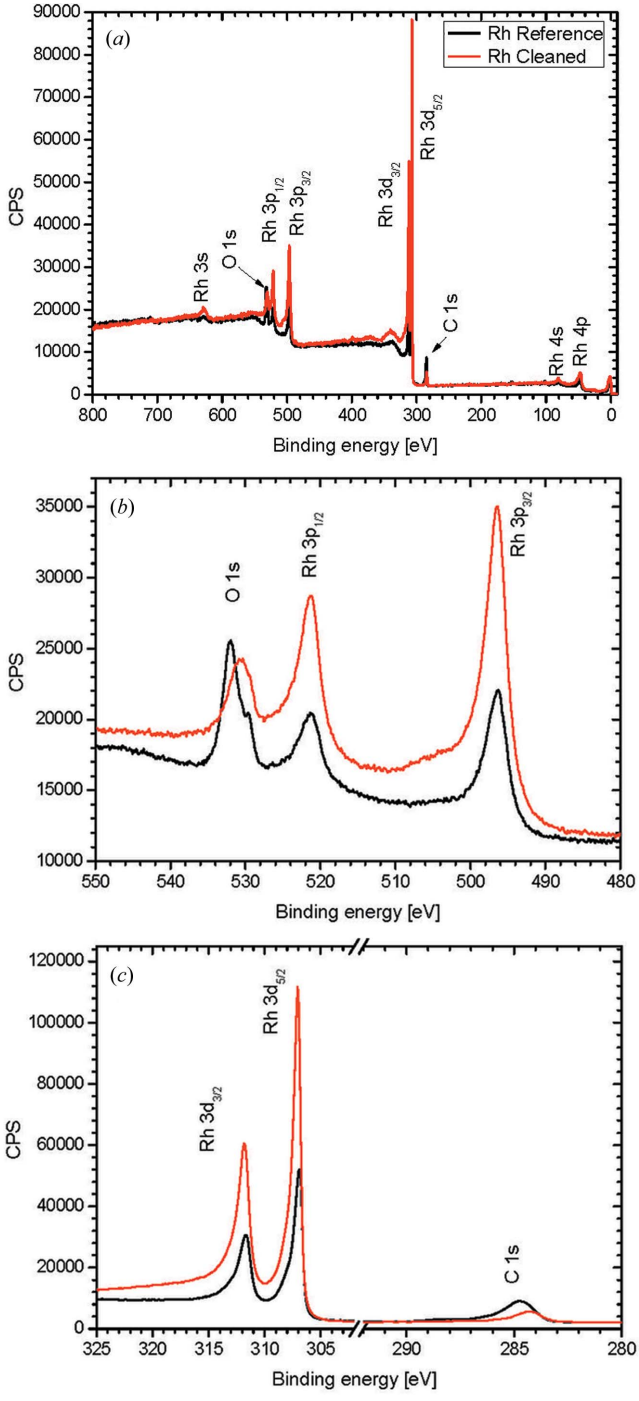

Figure 16
XPS spectra from a pristine Rh foil (black lines) as well as from a Rh foil after carbon contamination and subsequent hydrogen RF plasma cleaning using a GV10x ICP RF gun (red lines).

4.3.1. Discussion. The obvious differences in the plasma chemistry using either oxygen- or hydrogen-based feedstock gas mixtures have become apparent in the present study. Differences start with the different gas kinetics involved in the gas supply system (Blessing *et al.*, 2007) (*e.g.* due to the different gas viscosities of hydrogen and argon) and also encompass the different reactivity of oxygen *versus* hydrogen radicals.

Previous studies have already dealt with the difficulties associated with the transport of free hydrogen radicals in vacuum systems (Grubbs & George, 2006) as well as with the hydrogen RF plasma cleaning process. The former study did observe a pronounced recombination of hydrogen radicals into H_2 molecules that depends on the material composition of the vacuum chamber inside wall surfaces. The associated recombination coefficients are highest for stainless steel and lowest for quartz tubes (Grubbs & George, 2006). We attribute the low cleaning rate for a pure hydrogen feedstock gas (see Table 3) in conjunction with the observation of a temperature increase of the vacuum chamber wall materials just downstream of the plasma gun exit to the above exothermal hydrogen recombination process. This leads to a reduced concentration of free hydrogen radicals on their trajectory from the plasma gun to the location of the test crystal on the quartz microbalance to be cleaned. In this context, the increase in cleaning rate with the increasing admixture of argon into the feedstock can be interpreted as an embedding of the flow of hydrogen radicals within a neutral gas carrier matrix. This effectively reduces the interaction of the hydrogen radicals with the vacuum chamber wall material as well as among each other, thus increasing the carbon cleaning rate. Therefore, Ar as a feedstock gas admixture is not only beneficiary in view of facilitating plasma ignition due to its low breakdown voltage, but also by providing an inert transport carrier gas matrix for reactive gas species. In addition, and as already mentioned in the context of oxygen as well as hydrogen plasma cleaning in the previous sections, the excited Ar species also appear to play an active role in the conversion of carbon into volatile species as is the case in industrial processes such as the thermal plasma jet conversion pyrolysis of coal into acetylene (Fridman, 2008).

The highest cleaning rates shown in Table 4 can be compared with similar data obtained by Graham *et al.* (2002) using either an RF discharge or a hot tungsten filament (Graham *et al.*, 2003) set-up as sources for hydrogen radicals (see Table 5).

Table 5
Cleaning rates in Å h^{-1} for different hydrogen plasma cleaning processes from the literature as well as from the present study.

Angles are defined as those between the source axis and the sample normal.

Reference	Cleaning rate	Feedstock gas	Pressure	Power	Plasma source	Radical handling	Source distance /angle
Graham *et al.* (2002)	10 Å h^{-1}	H_2	0.02 mbar	100 W	RF cell	None	51 cm/0°
Graham *et al.* (2003)	60 Å h^{-1}	H_2	0.001 mbar	378 W	Hot W filament including quartz tube	Quartz tube	20 cm/0°
This work	102 Å h^{-1}	7% H_2, 93% Ar	0.0015 mbar	99 W	GV10x RF Downstream Asher	Inert carrier gas	38 cm/90°

The above comparison points out the importance of gas transport when it comes to the adequate handling of reactive species such as hydrogen radicals during the plasma processes [see the low cleaning rate from Graham *et al.* (2002)]. This has already been pointed out in many studies (Grubbs & George, 2006; Graham *et al.*, 2003; Motai *et al.*, 2007) where the use of quartz tubes for the gas transport from the source to the application has been emphasized. In addition to the apparent advantages of Ar as a carrier gas as compared with quartz tube ducts when comparing the present cleaning rate with the corresponding result from Graham *et al.* (2003), the enhanced cleaning rate obtained in the present study also corroborates another useful operation principle of the Downstream Asher, where the gas jet produced by the pressure difference between the plasma volume and the cleaning chamber allows for an efficient transport of the chemically active species.

The obviously low cleaning rate as the main disadvantage of hydrogen plasma cleaning as compared with the oxygen plasma process is largely compensated by the uncompromised and even improved chemical characteristics of the optical surfaces by this type of cleaning process. This relieves the restrictions as imposed by VUV-generated ozone and oxygen RF plasma processes regarding the choice of coating materials for the reflective optical surfaces for soft X-ray beamlines (so far limiting the choice to Au and Pt) and thus allowing the designer of the beamline optics to select the most appropriate material according to optical criteria.

5. Summary and outlook

In the present study an attempt has been made to systematize and optimize some of the approaches that have been used so far regarding the *in situ* low-pressure RF plasma cleaning of synchrotron beamline optics. The main results are the following:

(i) Capacitive coupled 'traditional' low-pressure RF plasma sources appear to be less efficient and thorough than inductively coupled plasma sources in terms of cleaning rates and an as low as possible amount of residual surface carbon atoms when using oxygen as a feedstock gas.

(ii) From the optical emission spectra it is clear that the above finding is due to the higher production rate of neutral $O^{\bullet}$ radicals as well as due to the radical transport associated with the dynamic gas supply mode in the case of the ICP gun (as compared with the CCP guns).

(iii) Oxygen plasma cleaning using an ICP gun does not have a detrimental influence on the surface micro-roughness of the cleaned object, but unavoidably leads to the oxidation of non-noble reflective metal coatings such as Ni as well as to the oxidation of a noble metal such as Rh at room temperature. So far, from the metallic coatings explored in this study only Au is not chemically affected by oxidation processes.

(iv) Hydrogen/argon feedstock gas mixtures represent a viable alternative to oxygen/argon gas mixtures since all the reflective metals investigated so far (Ni, Rh and Au) show a clear improvement in terms of surface cleanliness as compared with the corresponding pristine metals without chemically modifying the reflective metal coating itself. In addition, no change of the surface morphology or micro-roughness could be observed.

(v) The drawback of the cleaning process with hydrogen/argon feedstock gas mixtures as compared with oxygen/argon driven processes consists of a cleaning rate which is reduced by a factor of about seven. Nevertheless, the basic operation Downstream Asher

Table 6
Summary of XPS binding energies (all in eV) from the core level spectra shown in this work.

Material	Core level line	Unprocessed reference foil	O_2/Ar plasma cleaned foil	H_2/Ar plasma cleaned foil
Au foil	Au $4f_{7/2}$	84.0	84.0	83.9
	Au $4f_{5/2}$	87.7	87.7	87.55
	Au $4d_{5/2}$	335.0	335.0	334.95
	Au $4d_{3/2}$	353.3	353.3	353.25
	Au $4p_{3/2}$	547.0	547.0	546.7
	Au $4p_{1/2}$	642.0	642.0	–
	O1*s*	531.0	531.0	532.0
	C1*s*	284.7	284.5	284.6
Ni foil	Ni $2p_{3/2}$ (metal)	852.8	–	852.6
	Ni $2p_{1/2}$ (metal)	870.0	–	870.0
	Ni $2p_{3/2}$ (oxide) main, satellite	856.5, 861.8	856.2, 861.6	~855.5, ~861.0
	Ni $2p_{1/2}$ (oxide) main, satellite	874.2, 880.9	873.8, 880.1	~873.5, ~880.1
	O1*s* (main, shoulder)	532.0, 530.0	531.5, 530.0	531.8, 529.6
	C1*s* (main, shoulder)	285.5, 289.5	285.0, 288.5	285.0, 288.8
Rh foil	Rh $3d_{5/2}$	307.7	308.0	307.1
	Rh $3d_{3/2}$	312.0	312.5	311.9
	Rh $2p_{3/2}$	496.5	497.5	496.4
	Rh $2p_{1/2}$	521.5	522.0	521.3
	O1*s*	531.5	530.0	530.6
	C1*s*	284.7	284.7	284.3

principle of the ICP RF gun still warrants an acceptable cleaning time of carbon contamination layers.

(vi) None of the cleaning processes applied in the present study led to a contamination of the metal surfaces with foreign metals from, for example, the CCP or ICP RF gun system. Nevertheless, CCP plasma sources in conjunction with the observed inherent negative DC bias voltage of up to several hundreds of DC volts are suspected of sputtering metallic contaminations, depending on the details of the geometrical arrangements between the plasma source and the surface to be cleaned. The lack of metallic contaminations for the CCP cleaning in the present study is very probably due to the (intended) lack of any direct line of sight between the RF CCP gun and the test objects to be cleaned.

Future pending developments regarding the *in situ* low-pressure RF plasma cleaning of synchrotron optics encompass end-point detection schemes such as (non-invasive) *in situ* ellipsometry in order to protect the optical surfaces from an undue excessive cleaning. First experiments on the oxygen plasma cleaning of Si optical surfaces indicate that excessive cleaning times (*i.e.* well beyond the time required for the carbon cleaning) result in contamination of the optical surfaces and/or a reduced reflectivity of the mirrors.

Last but not least, the present ICP RF guns will be scaled up in size and RF power in order to cope with the requirements of large-size optics and the associated vacuum chambers.

We acknowledge skilful technical assistance by M. Thomasset (Synchrotron Soleil, Gif-sur-Yvette), M. Dominguez (CRnE, UPC, Barcelona), G. Sauthier (ICN2, Bellaterra) and A. Goñi (ICMAB-CSIC, Bellaterra).

References

Abe, Y., Kato, K., Kawamura, M. & Sasaki, K. (2001). *Surf. Sci. Spectra*, **8**, 117–125.

Blessing, J. E., Ellefson, R. E., Raby, B. A., Brucker, G. A. & Waits, R. K. (2007). *J. Vac. Sci. Technol. A*, **25**, 167–186.

Crosswhite, H. M. (1972). Editor. *The Hydrogen Molecule Wavelength Tables of H. G. Dieke.* New York: Wiley-Interscience.

Eggenstein, F., Senf, F., Zeschke, T. & Gudat, W. (2001). *Nucl. Instrum. Methods Phys. Res. A*, **467–468**, 325–328.

Fridman, A. (2008). *Plasma Chemistry.* Cambridge University Press.

Galtayries, A. & Grimblot, J. (1999). *J. Electron Spectrosc. Relat. Phenom.* **98–99**, 267–275.

Gibson, J. H. (1985). MS Thesis, University of Minnesota, USA.

Graham, S., Steinhaus, C., Clift, M. & Klebanoff, L. (2002). *J. Vac. Sci. Technol. B*, **20**, 2393–2400.

Graham, S., Steinhaus, C., Clift, M., Klebanoff, L. & Bajt, S. (2003). *Proc. SPIE*, **5037**, 460–469.

Grubbs, R. K. & George, S. M. (2006). *J. Vac. Sci. Technol. A*, **24**, 486–496.

Johnson, E. D. & Garrett, R. F. (1988). *Nucl. Instrum. Methods Phys. Res. A*, **266**, 381–385.

Kurucz, R. (1995). CD-ROM No. 23, Harvard-Smithsonian Center for Astrophysics, USA.

Lieberman, M. A. & Lichtenberg, A. J. (2005). *Principles of Plasma Discharges and Materials Processing.* New York: Wiley-Interscience.

Mansour, A. N. & Melendres, C. A. (1994). *Surf. Sci. Spectra*, **3**, 263–270.

Miller, A. C. & Simmons, G. W. (1993). *Surf. Sci. Spectra*, **1**, 312–317.

Motai, K., Oizumi, H., Miyagaki, S., Nishiyama, I., Izumi, A., Ueno, T., Miyazaki, Y. & Namiki, A. (2007). *Proc. SPIE*, **6517**, 65170F.

NIST (1999). *NIST Atomic Spectra Database*, Version 2.0. National Institute of Standards and Technology, http://physics.nist.gov/cgi-bin/AtData/main_asd.

Pearse, R. W. B. & Gaydon, A. G. (1963). *The Identification of Molecular Spectra*, 3rd ed. London: Chapman and Hall.

Pearse, R. W. B. & Gaydon, A. G. (1976). *The Identification of Molecular Spectra*, 4th ed. New York: Wiley.

Rosenberg, R. A. & Crossley, D. B. (1988). *Nucl. Instrum. Methods Phys. Res. A*, **266**, 386–391.

Shpilman, Z., Gouzman, I., Lempert, G., Grossman, E. & Hoffman, A. (2008). *Rev. Sci. Instrum.* **79**, 25106.

Striganov, A. R. & Sventitskii, N. S. (1968). *Tables of Spectral Lines of Neutral and Ionized Atoms.* New York: IFI/Plenum.

Tolia, A. A., Smiley, R. J., Delgass, W. N., Takoudis, C. G. & Weaver, M. J. (1994). *J. Catal.* **150**, 56–70.

Wiese, W. L. *et al.* (1966, 1969). *Atomic Transition Probabilities*, Vols. I & II. Washington: NBSDS.